Carrier transport and optical properties of InGaNSQW with embedded AlGaN delta-layer

Park, JW; Kaneta, A; Funato, M; Kawakami, Y

Carrier Transport and Optical Properties of InGaN SQW With Embedded AlGaN δ-Layer

Jongwoon Park, Akio Kaneta, Mitsuru Funato, and Yoichi Kawakami

***Abstract*—We investigate the carrier transport and optical properties of a thick InGaN single quantum well (SQW) where an AlGaN δ-layer is embedded. By way of simulation, it is found that the carrier density distribution in the active region is more uniform in such a QW structure, compared to a double QW (DQW) configuration showing a discontinuity in the hole quasi-Fermi level due to the large effective mass of the holes along with the strong piezoelectric field. Through the photoluminescence (PL) measurements, we have shown that the PL peak energy varies depending sensitively on the δ-layer thickness, providing an extra degree of freedom in the wavelength-tuning control. In particular, such a QW structure is highly desired for long-wavelength emission as the wavelength tuning can be achieved with lower indium composition. The embedded δ-layer also increases the wave function overlap between holes and electrons, thereby shortening the PL lifetime. The results of PL measurements are shown to be consistent with the self-consistent numerical results. A possible application of the proposed QW structure is to the design of long-wavelength light-emitting diodes and laser diodes.**

***Index Terms*—AlGaN, carrier transport, delta layer, InGaN, photoluminescence, piezoelectric charge, wave function.**

I. Introduction

THE wide bandgap III–nitride semiconductor materials are of great importance for many semiconductor device applications in lighting [1], [2], full-color display, optical storage, medical applications [3], etc. Despite the tremendous efforts in the growth, the poor crystal quality due to high dislocation densities and the strong piezoelectric field effects induced by large lattice mismatch are still the main limiting factors for their applications [4], especially to InGaN-based long-wavelength (green and red) light-emitting devices that are highly demanded for full-color displays. For long-wavelength tuning, one has to inevitably increase the quantum-well (QW) thickness and/or the indium content. With thick QWs, however, we are faced with a situation where the strong piezoelectric field reduces dramatically the oscillator strength [5], resulting in a decrease of the internal quantum efficiency; whereas several defects such as V-defects, stacking faults, and dislocations [6] are parasitic in QWs with high indium content, causing high nonradiative recombination. Consequently, the threshold current density of laser diodes increases as the emission wavelength increases. Nakamura *et al.* [7] found that an InGaN-based QW structure with two QWs gave rise to the lowest threshold current for near 400-nm lasers. They also found [8] that for lasers with longer emission wavelength (>435 nm), a structure with only one QW [i.e., single QW (SQW)] showed the lowest threshold current density. The generation of lasing oscillation was not even feasible beyond 475 nm [9] due mainly to the deterioration of the crystal quality. Those defect centers appearing in light-emitting diodes (LEDs) also bring on high sensitivity of device performances to the temperature [10]. With increasing temperature, the decrease in output power for LED with a higher In composition in the multiple QW (MQWs) was higher than that of LED with a lower In content in the MQWs. To make matters worse, the carrier distribution over the QWs is highly nonuniform [11], [12] due to large valence-band offset and low mobility of the holes, which is also crucial for laser performance.

To overcome such pitfalls, we propose a novel QW structure based on a thick InGaN SQW in which an AlGaN δ-layer is embedded. We first investigate the carrier transport property of the QW structure by solving Poisson's equation and the drift-diffusion equation iteratively. We then analyze the optical [photoluminescence (PL)] properties of the QW structure by time-resolved PL (TRPL) spectroscopy. The effects of varying the In mole fraction of the QWs and the AlGaN δ-layer thickness are also investigated. For a systematic study, we have further solved the effective-mass Schrödinger equation. A numerical investigation of the band structure and material gain offers a clear understanding with regard to the optical behaviors of the QW structures. In the model, the strain effects of those wurtzite semiconductor materials are considered and the piezoelectric sheet charge density is incorporated in Poisson's equation so that the phenomena such as the tilt of the energy band, the spatial separation of electrons and holes, and the charge screening by the injected carriers are all captured. The composition distribution in the QWs is assumed to be homogeneous for simplicity.

This paper is organized as follows. In Section II, the numerical model for the simulation of III–nitride semiconductors is briefly described. Simulation and measurement results, e.g., the carrier transport, PL intensity, and PL decay dynamics, are presented and analyzed in Section III. Finally, a conclusion is drawn in Section IV.

II. Model and Implementation

Built-in interface charge due to spontaneous and piezoelectric polarizations in the GaN material system is incorporated in Poisson's equation written as [13]

$$\nabla \cdot (\varepsilon \nabla \psi) = -q(p - n + N_D - N_A) - \rho_{\text{pol}} \quad (1)$$

Manuscript received March 1, 2006; revised June 20, 2006. This work was supported in part by the Kyoto University-Venture Business Laboratory (KU-VBL) Project, Japan.

The authors are with the Department of Electronic Science and Engineering, Kyoto University, Kyoto 615-8510, Japan (e-mail: pjwup@fujita.kuee.kyoto-u.ac.jp; kaneta@fujita.kuee.kyoto-u.ac.jp; funato@kuee.kyoto-u.ac.jp; kawakami@kuee.kyoto-u.ac.jp).

Digital Object Identifier 10.1109/JQE.2006.881722

where the variable ψ represents the electrostatic potential, n and p the electron and hole densities, respectively, N_D and N_A the donor and acceptor impurity concentrations, respectively, and $\rho_{\rm pol}$ the polarization charge density given as

$$\rho_{\rm pol} = -\frac{\partial}{\partial z}\left[e_{33}\varepsilon_{\perp}(x) + 2e_{31}\varepsilon_{\parallel}(x) + P_{\rm sp}(x)\right] \tag{2}$$

where

$$\varepsilon_{\parallel}(x) = \frac{a_{sub} - a(x)}{a(x)} \text{ and } \varepsilon_{\perp}(x) = -2\varepsilon_{\parallel}(x)\frac{C_{13}}{C_{33}} \tag{3}$$

defined as the strain components parallel and perpendicular to the QW plane, respectively. e_{ij} are the coefficients of the piezoelectric tensor and $P_{\rm sp}(x)$ is the spontaneous polarization. All the parameter values are adopted from [13]. Equation (1) is solved by Newton–Raphson iteration on a finite difference approximation [14], [15]. The piezoelectric field generates the sheet charge density at the interface between a QW and a barrier. By increasing the injection current, however, the piezoelectric field is cancelled out by the free-carrier-induced field [16]. Such a charge screening effect is naturally captured in the model.

The carrier transport in the active region can be described by the following drift-diffusion equation for electrons and holes [15]

$$\frac{\partial n}{\partial t} = \frac{1}{q}\nabla\cdot(-q\mu_n n\nabla\phi_n) + G - R \tag{4a}$$

$$\frac{\partial p}{\partial t} = \frac{1}{q}\nabla\cdot(-q\mu_p p\nabla\phi_p) + G - R \tag{4b}$$

$$n = n_i \exp\left[\{(\psi+\theta-\gamma_n) - \phi_n\}/V_T\right] \tag{4c}$$

$$p = n_i \exp\left[\{\phi_p - (\psi+\theta-\gamma_p)\}/V_T\right] \tag{4d}$$

where the variable μ_n denotes the electron mobility, μ_p the hole mobility, and ϕ_n and ϕ_p the quasi-Fermi potentials for electrons and holes, respectively. All the other parameters are the same as defined in [15] where a detailed implementation is also introduced. To facilitate the numerical calculation, the differential equation (4) is discretized with the box integral discretization scheme [15]. The band-offset ratio $(\Delta E_c/\Delta E_v)$ of InGaN–GaN and AlGaN–GaN is assumed to be 0.7/0.3 [17] and 0.67/0.33 [11], [18], respectively. The bandgap energy and the material parameter values such as the refractive index and the electron and hole mobilities used in our simulation are the same as presented in [18]. The effective masses of electrons and holes are adopted from [11].

For the calculation of the band structure and material gain of the QW structure, we have also solved the effective-mass Schrödinger equation [19]–[21] expressed as for the valence band

$$\sum_{j=1}^{6}\left(H_{ij} + \delta_{ij}E^v(z)\right)\varphi_m^{(j)}(z) = E_m^v\varphi_m^{(i)}(z), \quad i = 1,2,\ldots,6 \tag{5}$$

with the 6×6 effective-mass Hamiltonian defined as

$$H_{6\times 6} = \begin{bmatrix} H^U & 0 \\ 0 & H^L \end{bmatrix} \tag{6}$$

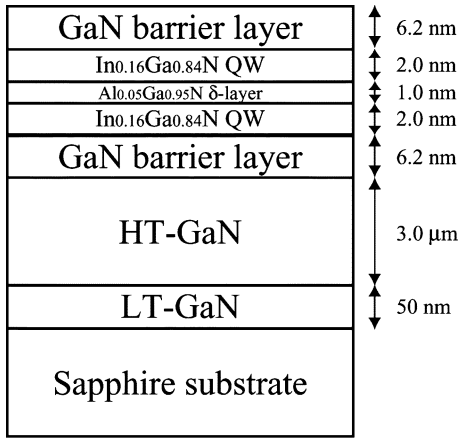

Fig. 1. Schematic layer structure of the sample with the AlGaN δ-layer grown by MOVPE.

where H^U and H^L are 3×3 matrices with the relation of $H^U = (H^L)^*$, and

$$H^U = \begin{bmatrix} F & K_t & -iH_t \\ K_t & G & \Delta - iH_t \\ iH_t & \Delta + iH_t & \lambda \end{bmatrix} \tag{7}$$

$$F = \Delta_1 + \Delta_2 + \lambda + \theta$$

$$G = \Delta_1 - \Delta_2 + \lambda + \theta, \quad \Delta = \sqrt{2}\Delta_3$$

$$\lambda = \frac{\hbar^2}{2m_0}\left(A_1k_z^2 + A_2k_t^2\right) + D_1\varepsilon_{zz} + D_2(\varepsilon_{xx}+\varepsilon_{yy})$$

$$\theta = \frac{\hbar^2}{2m_0}\left(A_3k_z^2 + A_4k_t^2\right) + D_3\varepsilon_{zz} + D_4(\varepsilon_{xx}+\varepsilon_{yy})$$

$$K_t = \frac{\hbar^2}{2m_0}A_5k_t^2, \quad H_t = \frac{\hbar^2}{2m_0}A_6k_zk_t \tag{8}$$

for the conduction band

$$\left[\frac{\hbar^2}{2}\left(\frac{k_t^2}{m_e^t} + \frac{k_z^2}{m_e^z}\right) + E^c(z)\right]\varphi_n(z) = E_n^c\varphi_n(z). \tag{9}$$

The valence $(E^v(z))$ and conduction $(E^c(z))$ band edge profiles appearing in (5) and (9) are obtained after solving Poisson's equation (1) and conventional drift-diffusion equation (4). Therefore, the effect of free-carrier screening is also considered in the calculation of quantum energy levels. To calculate the energy levels of the valence (E_m^v) and conduction (E_n^c) bands and the associated wave functions of $\varphi_m(z)$ and $\varphi_n(z)$, (5) and (9) are spatially discretized with a standard central differencing scheme and solved with the inverse power method [22]. All the parameter values and more detailed descriptions are available in [19]–[21].

The optical gain is calculated by [20], [21]

$$g(\hbar w) = g_{\rm sp}(\hbar w)\left[1 - \exp\left(\frac{\hbar w - \Delta F}{kT}\right)\right] \tag{10a}$$

$$g_{\rm sp}(\hbar w) = \frac{q^2\pi}{n_r c\varepsilon_0 m_0^2 w L_w}\sum_{\sigma=U,L}\sum_{n,m}\int\frac{k_t dk_t}{2\pi}\left|(M_e)_{nm}^{\sigma}(k_t)\right|^2 \times f_n^c(k_t)\left[1 - f_{\sigma,m}^v(k_t)\right] \times \frac{\hbar\gamma/\pi}{\left[E_{\sigma,nm}^{cv}(k_t) - \hbar w\right]^2 + (\hbar\gamma)^2} \tag{10b}$$

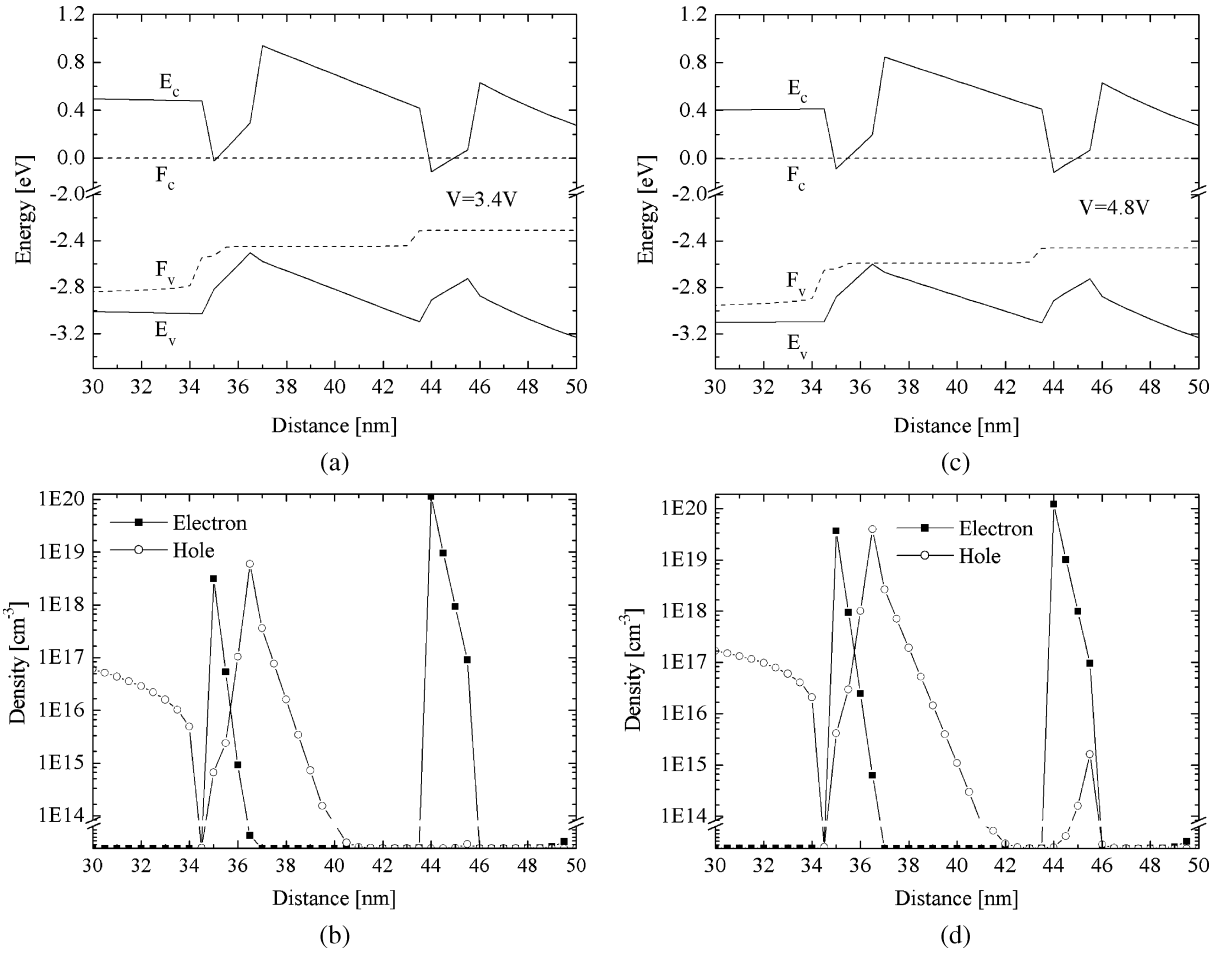

Fig. 2. (a) Energy band diagram and carrier density distribution at 3.4 V and (b) at 4.8 V (c)–(d) in the active region consisting of two 2-nm-thick $In_{0.16}Ga_{0.84}N$ QWs separated by a 7-nm-thick $Al_{0.05}Ga_{0.95}N$ barrier.

with the TE-polarized matrix element express as

$$|(M_x)^{\sigma}_{nm}(k_t)|^2 = \frac{|\langle S|p_x|X\rangle|^2}{4}\left\{\left\langle \varphi_n|\varphi^{(1)}_m\right\rangle^2 + \left\langle \varphi_n|\varphi^{(2)}_m\right\rangle^2\right\}, \quad \text{for } \sigma = U \tag{11a}$$

$$|(M_x)^{\sigma}_{nm}(k_t)|^2 = \frac{|\langle S|p_x|X\rangle|^2}{4}\left\{\left\langle \varphi_n|\varphi^{(4)}_m\right\rangle^2 + \left\langle \varphi_n|\varphi^{(5)}_m\right\rangle^2\right\}, \quad \text{for } \sigma = L. \tag{11b}$$

All the variables appearing in (10) and (11) are the same as defined in [20] and [21].

In our model based on the conventional bulk carrier transport equations [15], the effect of quantum carrier capture [23] is neglected. Therefore, the carrier density in the lowest bound states calculated by it could be a little overestimated. Even so, we have used the bulk carrier transport model combined with the effective mass Schrödinger equation, since the effect of the delta-layer on the overall carrier transport, especially in the presence of piezoelectric charges, is our main concern in this work. As mentioned, this model is indeed capable of capturing the piezoelectric field effect and the screening effect as well, which are key issues in GaN-based semiconductor devices.

III. Results and Discussion

InGaN–GaN SQW samples were grown on (0001) sapphire substrates by metal–organic vapor phase epitaxy (MOVPE). In the QW structure shown in Fig. 1, a 1-nm-thick AlGaN δ-layer is embedded in the center of a 5-nm-thick InGaN QW (i.e., 2 nm $In_{0.16}Ga_{0.84}N$ – 1 nm $Al_{0.05}Ga_{0.95}N$ – 2 nm $In_{0.16}Ga_{0.84}N$). The indium composition and overall well thickness are measured to be 16% and 4 nm (= 2 nm – $In_{0.16}Ga_{0.84}N$ + 2 nm – $In_{0.16}Ga_{0.84}N$), respectively, by the x-ray rocking curve analysis. The AlGaN δ-layer was grown at the same growth temperature as the InGaN QW layer. Low (740 °C) and high (1320 °C) temperature deposited GaN buffer layers were used to enhance the quality of upper-grown barriers and QWs. The samples have an undoped SQW that is sandwiched between 6.2-nm-thick GaN barriers. In the PL measurement, they were excited with 1.5 ps pulses from a frequency-doubled Ti:sapphire laser. The laser wavelength is 400 nm and the repetition rate is 80 MHz. All measurements were carried out at 13 K.

A. Carrier Transport Property

The carrier transport to the QWs plays an important role in the spontaneous emission efficiency and thus laser performance. Ignoring the piezoelectric charges in the simulation [11], the hole

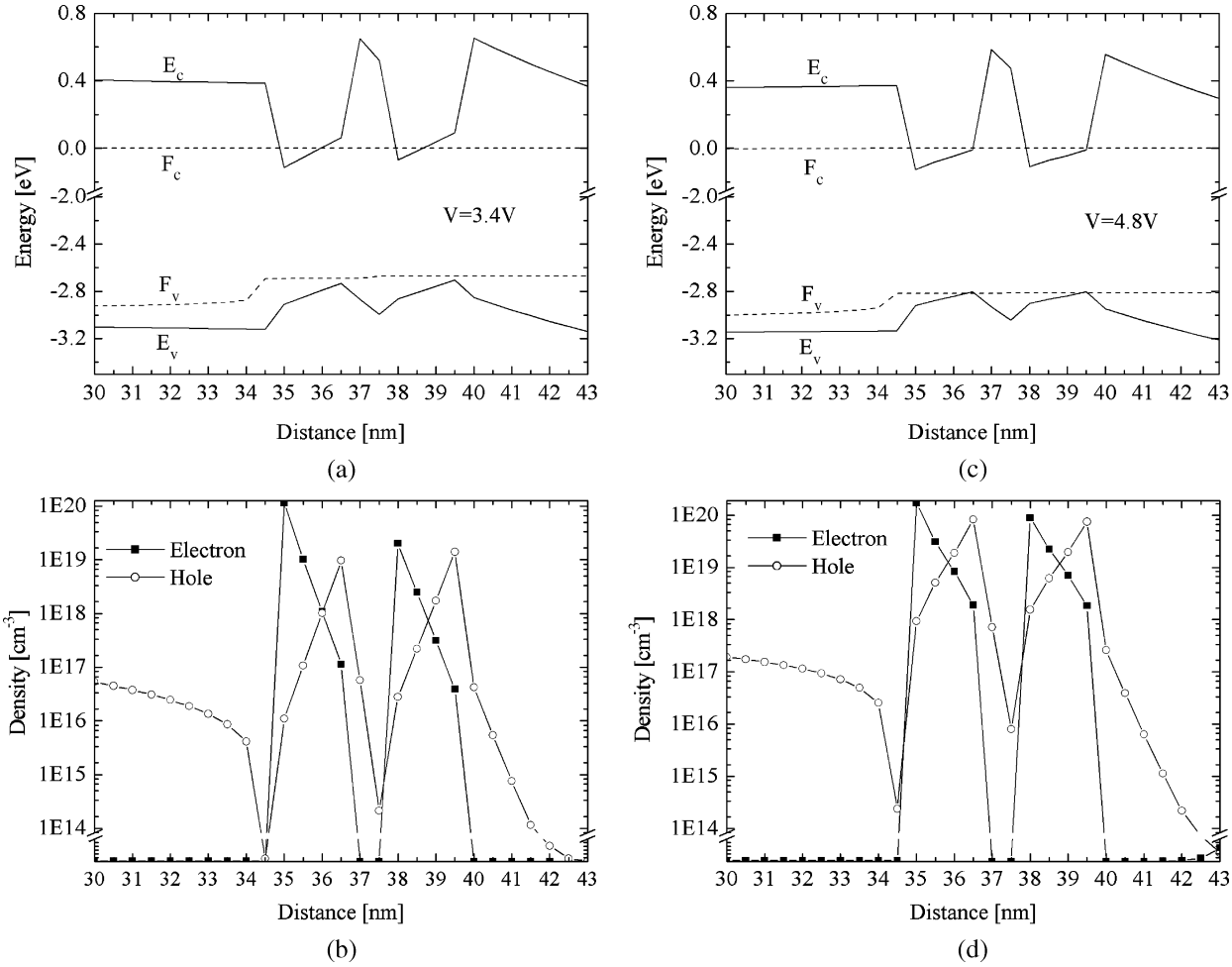

Fig. 3. (a) Energy band diagram and carrier density distribution at 3.4 V and (b) at 4.8 V (c)–(d) in the active region with the 1-nm-thick $Al_{0.05}Ga_{0.95}N$ δ-layer embedded in the 5-nm-thick $In_{0.16}Ga_{0.84}N$ QW.

distribution over three $In_{0.25}Ga_{0.75}N - In_{0.02}Ga_{0.98}N$ QWs for 461-nm lasers is very uniform. In the presence of piezoelectric charges, however, we have found that the holes have difficulty in entering the QWs due to their large effective mass. Consequently, the hole distribution is highly inhomogeneous with lower concentration in the n-side QW (the right-hand side of the diagram) as evident in Fig. 2, showing the energy band profile and carrier distribution in the active region consisting of two 2-nm-thick $In_{0.16}Ga_{0.84}N$ QWs separated by a 7-nm-thick $Al_{0.05}Ga_{0.95}N$ barrier. We can clearly see the discontinuity in the hole quasi-Fermi level (F_v) in both QWs, implying a difficulty in the hole transport. Due to the large conduction band offset, the electron distribution is also nonuniform with lower concentration in the p-side QW (the left-hand side of the diagram). The partial charge screening effect by the injected carriers is thus observed only in the n-side QW. Such an inhomogeneous carrier distribution could be one of the main reasons that the lowest threshold current density is achieved when the number of QWs is only one (i.e., SQW) for the lasing wavelengths longer than 435 nm [8], [12]. If one has to use a thin SQW for the reason, however, the temperature and the current overflow in the active region would be issues for high current injection [12], since the carriers are overcrowded in the active region and the confinement factor of the SQW is very low, which is in proportion to the active layer thickness.

In the proposed QW structure where a 1-nm-thick AlGaN δ-layer is embedded in the center of a 5-nm-thick InGaN SQW, however, the discontinuity in F_v has disappeared as shown in Fig. 3. As a result, highly uniform carrier distribution is observed. Furthermore, the charge screening effect is more pronounced in both QWs. It is apparent that the carrier distribution is getting inhomogeneous with increasing emission wavelength due to increased indium content (i.e., increased band offset). From the simulation results, therefore, it is our natural expectation that the threshold current density may be much lowered for long-wavelength lasers based on such a QW structure, since the internal quantum efficiency of spontaneous emission may increase by virtue of the uniform carrier distribution in the active region. In addition, one may be released from the concerns related to the temperature and the current overflow that could be issues in a SQW structure unavoidably employed for long-wavelength emission under high bias current.

B. Optical Properties: PL Intensity and PL Decay Dynamics

In the proposed QW structure, a coupling between QWs exists in the sense that the δ-layer can be regarded as a very

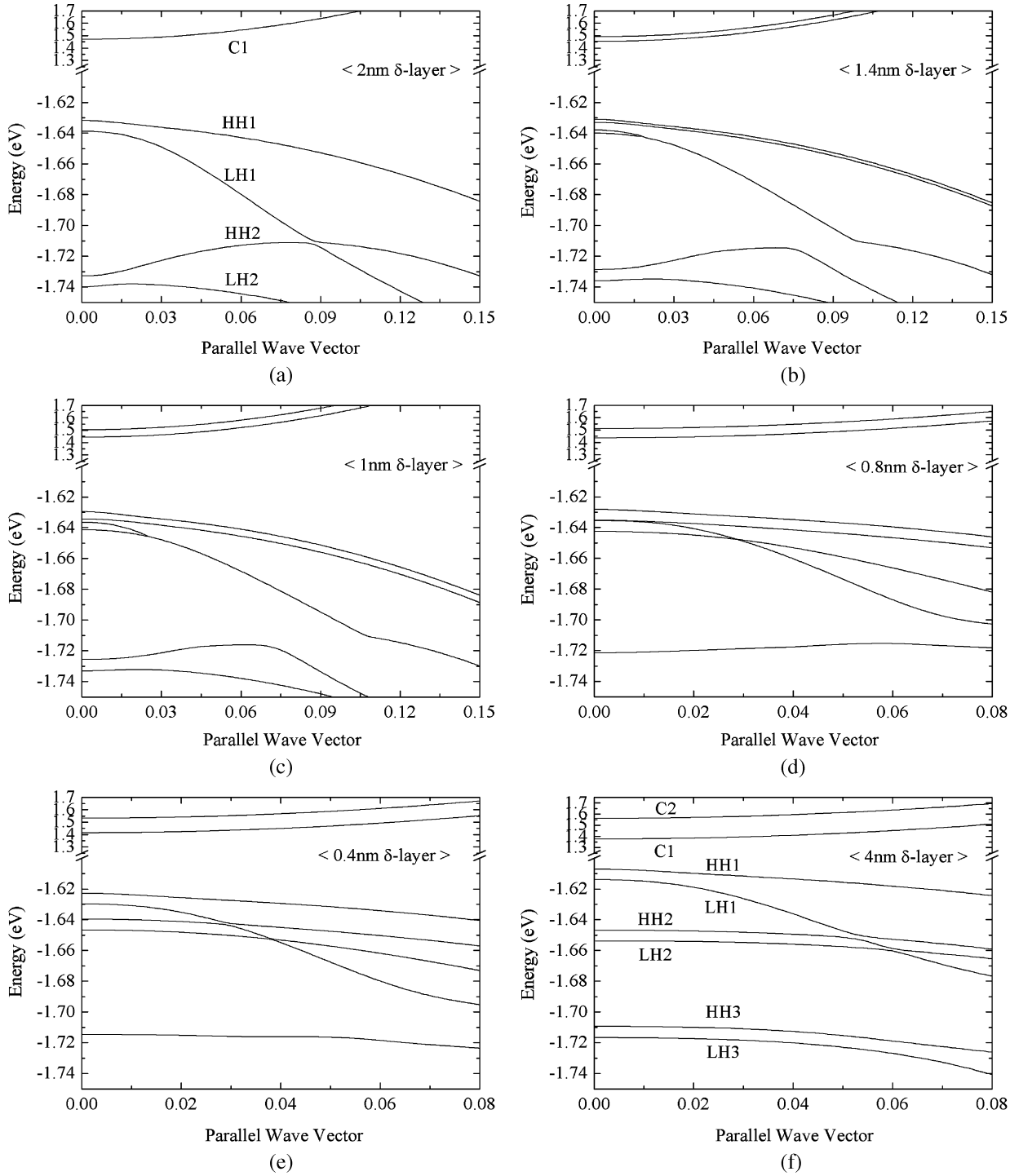

Fig. 4. In-plane dispersion of conduction and valence subbands of 2-nm-thick $In_{0.16}Ga_{0.84}N$ SQW, $In_{0.16}Ga_{0.84}N$ QWs with 0.4-, 0.8-, 1.0-, and 1.4-nm-thick $Al_{0.05}Ga_{0.95}N$ δ-layers, and 4-nm-thick $In_{0.16}Ga_{0.84}N$ SQW.

thin barrier. Namely, the QW structure is similar to a DQW system with a very thin AlGaN barrier. In order to perceive the optical behaviors of such a QW structure, we have first calculated the in-plane subband dispersion for different δ-layer thicknesses and presented the results in Fig. 4. For a comparative study, we have also calculated the band structures of 2-nm-thick and 4-nm-thick SQWs without a δ-layer. As seen in Fig. 4, the lowest conduction subband (C1) of the 2-nm-thick SQW is split into two subbands in the QW with the δ-layer. The separation increases further with decreasing δ-layer thickness. In the end, when the δ-layer thickness is zero, those separated subbands become the subbands (C1 and C2) of the 4-nm-thick SQW, a phenomenon known as the effect of a well coupling. Similar behavior also appears in the valence band; namely, those four subbands split from the HH1 and LH1 subbands of the 2-nm-thick SQW eventually become the HH1, LH1, HH2, and LH2 subbands of the 4-nm-thick SQW. Therefore, the transition energy of the

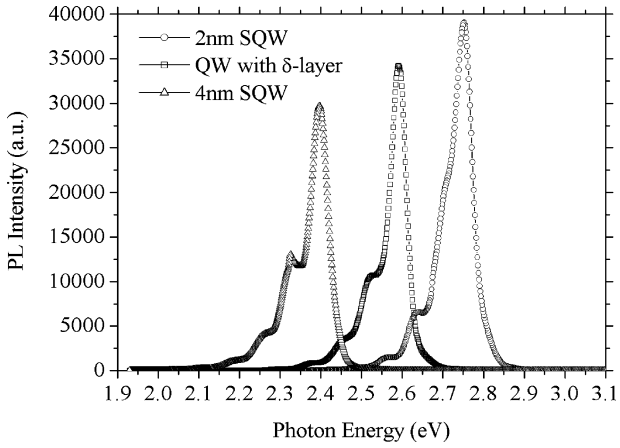

Fig. 5. Low-temperature (13 K) continuous-wave PL spectra of nominally undoped 4-nm-thick $In_{0.16}Ga_{0.84}N$ SQW ($-\triangle-$), $In_{0.16}Ga_{0.84}N$ (2 nm) $-$ $Al_{0.05}Ga_{0.95}N$ (1 nm)$-$$In_{0.16}Ga_{0.84}N$ (2 nm) QW ($-\square-$), and 2-nm-thick $In_{0.16}Ga_{0.84}N$ SQW ($-\bigcirc-$).

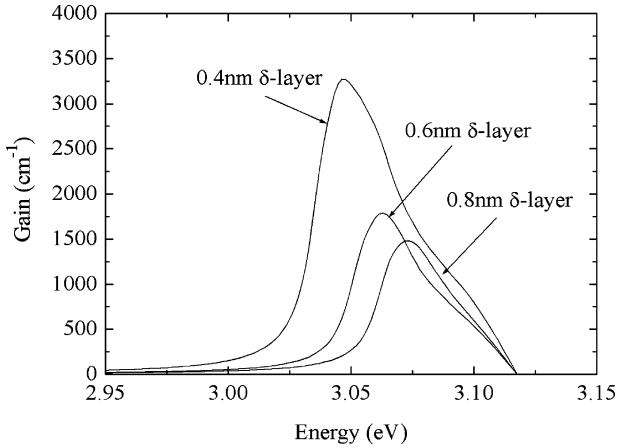

Fig. 6. Material gain spectra for different δ-layer thicknesses in the absence of piezoelectric charge when the carrier density is equal to 3×10^{19} cm^{-3}.

QW with the δ-layer always lies between or is rather bounded by the ones of those 2-nm-thick and 4-nm-thick SQWs. This numerical result is consistent with the measured one in Fig. 5, showing the low-temperature luminescence spectra of 4-nm-thick $In_{0.16}Ga_{0.84}N$ SQW, $In_{0.16}Ga_{0.84}N(2\text{ nm}) - Al_{0.05}Ga_{0.95}N(1\text{ nm})-In_{0.16}Ga_{0.84}N(2\text{ nm})$ QW, and 2-nm-thick $In_{0.16}Ga_{0.84}N$ SQW. As expected, the PL peak energy ($= 2.591$ eV, $\lambda = 478.48$ nm) of the QW with the δ-layer lies between that ($= 2.396$ eV, $\lambda = 517.36$ nm) of the 4-nm-thick SQW and that ($= 2.752$ eV, $\lambda = 450.48$ nm) of the 2-nm-thick SQW. We can, therefore, go on from these to conclude that one can tune the desired PL peak wavelength (energy) by adjusting the δ-layer thickness within the wavelength range decided by those 2-nm-thick (half-thick) and 4-nm-thick (same-thick) SQWs. One can also see from Fig. 5 that the PL efficiency is dependent on the δ-layer thickness. We shall return to this point later with simulation and experiment data. Based on the calculated band structures in Fig. 4, we have further computed the material gain spectra for different δ-layer thicknesses. As shown in Fig. 6, the material gain increases and the gain peak wavelength is red-shifted for a given carrier density as the δ-layer thickness decreases. This is ascribed to the fact that the lowest conduction (C1) and valence (HH1) subbands shift in such a way that they become close to the quasi-Fermi levels and thus the C1-HH1 transition energy is reduced with decreasing δ-layer thickness as evident in Fig. 4.

Fig. 7(a) shows the calculated energy band diagram and the lowest subband wave function of a 5-nm-thick $In_{0.16}Ga_{0.84}N$ SQW sandwiched between 10-nm-thick GaN barriers. Due to the spatial separation between the electrons and holes by the strong piezoelectric field, it is clearly seen that the wave function overlap between them is considerably decreased. However, it can be increased by the δ-layer embedded in the center of the SQW as depicted in Fig. 7(b). The electron wave function is further extended toward the n-side (the right-hand side of the diagram) and the hole wave function to the p-side of the QW. As a result, the PL efficiency has been increased as evident in Fig. 5 and the PL lifetime is expected to shorten since the transition probability increases. This is further supported by the luminescence decay dynamics in Fig. 8 measured at the emission peaks in the spectra (in Fig. 5) by TRPL spectroscopy. Through a curve fitting with $y = A_1 \exp(-(t/\tau_1)) + A_2 \exp(-(t/\tau_2))$, the PL lifetime ($\tau_1$) of 4-nm-thick $In_{0.16}Ga_{0.84}N$ SQW, $In_{0.16}Ga_{0.84}N(2\text{ nm}) - Al_{0.05}Ga_{0.95}N(1\text{ nm})-In_{0.16}Ga_{0.84}N(2\text{ nm})$ QW, and 2-nm-thick $In_{0.16}Ga_{0.84}N$ SQW is estimated to be 450, 104, and 13.2 ns, respectively. A drop (450 $\rightarrow$ 104 ns) in the PL lifetime is purely by the embedded δ-layer. As A_2 is nearly ten times smaller than A_1, the effect of the slow decay term τ_2 is negligible. Similar behavior observed in the PL spectra also appears in the luminescence decay dynamics; namely, the PL lifetime of the QW structure varies depending on the δ-layer thickness within the lifetime range determined by those 2-nm-thick (half-thick) and 4-nm-thick (same-thick) SQWs.

It would be more desirable to make a direct comparison at the same PL peak wavelength. To this end, we have so increased the In mole fraction of the 2-nm-thick SQW and the QW with the δ-layer as to emit the light around the green wavelength of 520 nm. In fact, the measured result in Fig. 5 gives us a hint that the QW structure with the δ-layer requires lower indium composition for long-wavelength tuning. Through the x-ray rocking curve analysis, the indium content of the QW with the δ-layer grown at 990 °C is shown to be about 5% lower than that of the 2-nm-thick SQW at 950 °C. Fig. 9(a) shows the PL decay dynamics measured around the emission peak of 520 nm. Little change is observed in the PL lifetime of the 2-nm-thick SQW (almost no change from the one in Fig. 8) due most likely to its very small thickness. It is likely that an increase in strain-induced piezoelectric charge does not affect the PL decay dynamics of a thin QW much. However, the deterioration of crystal quality would be much pronounced due to high indium composition, which is the root cause for high threshold current density of long-wavelength lasers [7]–[9]. This could also be the limiting factor for employing a thin SQW structure for long-wavelength emission, besides the aforementioned issues such as the temperature and the current overflow in the QW region. On the other hand, the PL lifetime of the QW with the δ-layer is increased to 254 ns, but still much shorter than that of the 4-nm-thick SQW.

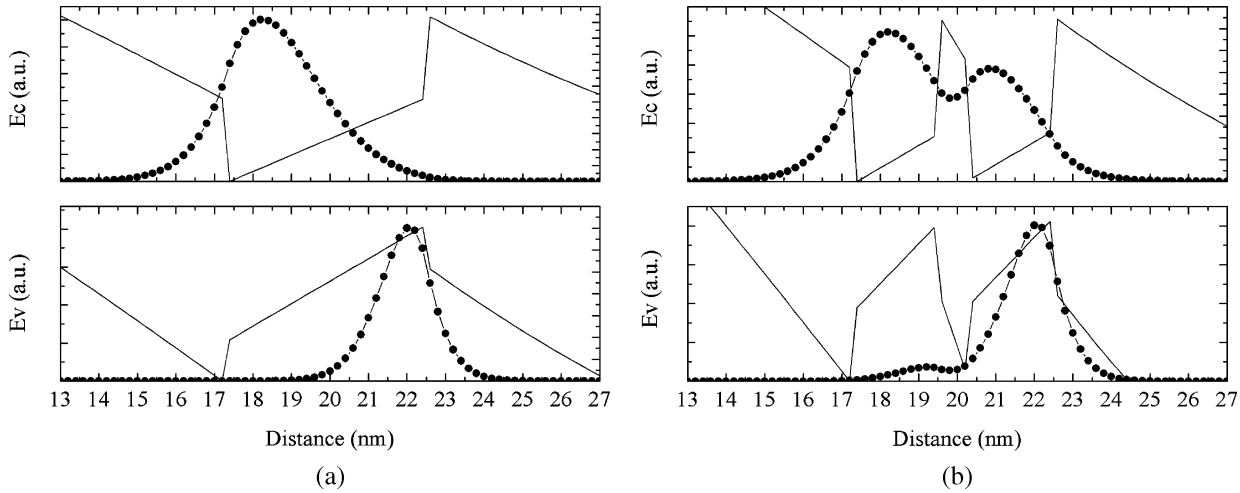

Fig. 7. Energy band diagram and wave function of (a) 5-nm-thick $In_{0.16}Ga_{0.84}N$ SQW and (b) $In_{0.16}Ga_{0.84}N$ (2 nm) $-$ $Al_{0.05}Ga_{0.95}N$ (1 nm $\delta-$layer) $-$ $In_{0.16}Ga_{0.84}N$ (2 nm) QW sandwiched between 10-nm-thick GaN barriers at zero bias current.

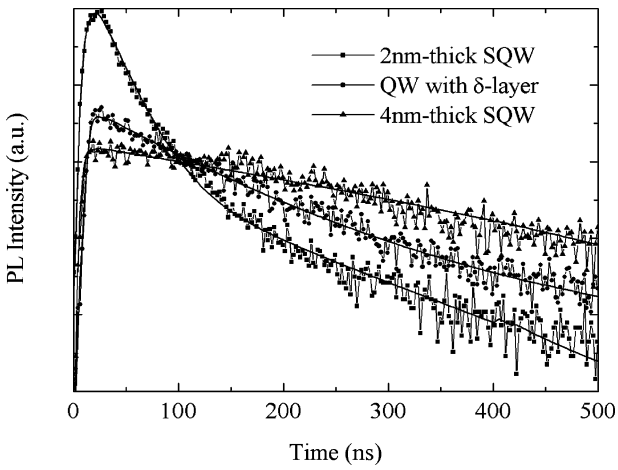

Fig. 8. Logarithmic plot of PL decay dynamics of nominally undoped 2-nm-thick $In_{0.16}Ga_{0.84}N$ SQW, $In_{0.16}Ga_{0.84}N$ (2 nm) $-$ $Al_{0.05}Ga_{0.95}N$ (1 nm)$-$$In_{0.16}Ga_{0.84}N$ (2 nm) QW, and 4-nm-thick $In_{0.16}Ga_{0.84}N$ SQW.

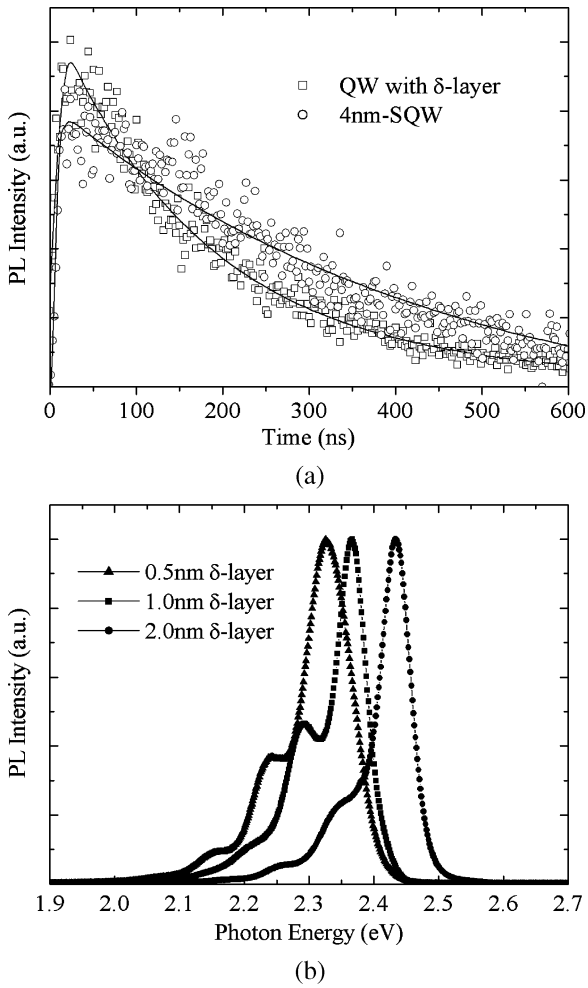

Fig. 9. Low-temperature (13 K) (a) PL decay dynamics of the 4-nm-thick SQW and the QW with the δ-layer and (b) continuous-wave PL spectra for different δ-layer thicknesses in the green wavelength region.

To investigate the effect of the δ-layer thickness on the emission peak, we have grown more samples emitting photons with the green PL peak energies (i.e., in the green wavelength region) and measured their PL spectra as shown in Fig. 9(b). The PL peak energy of the QWs with 0.5-, 1-, and 2-nm-thick δ-layers is measured to be 2.325 eV ($\lambda = 533.3$ nm), 2.366 eV ($\lambda = 523.9$ nm), and 2.433 eV ($\lambda = 509.6$ nm), respectively. In agreement with a conclusion drawn earlier in this section, the transition energy (PL peak wavelength) of the QW structure is reduced (increased) with decreasing δ-layer thickness.

IV. Conclusion

We have investigated the carrier transport and optical properties of a thick InGaN SQW where an AlGaN δ-layer is embedded. It has been demonstrated by way of simulation that a difficulty in the hole transport is dramatically reduced in the QW structure with the δ-layer, possibly enhancing the internal quantum efficiency of spontaneous emission and thus reducing the threshold current density of long-wavelength lasers based on such a QW structure. The PL peak energy depends sensitively on the δ-layer thickness, which offers an extra degree of freedom in emission wavelength tuning. We have also addressed that

the QW with the δ-layer needs a smaller amount of indium for long-wavelength tuning compared to the half-thick SQW, a feature highly desired for the design of long-wavelength light-emitting devices. Due to the increased wave function overlap by the embedded δ-layer, the QW structure also has shorter PL lifetime compared to the same-thick SQW.

REFERENCES

[1] S. C. Jain, M. Willander, J. Narayan, and R. V. Overstraeten, "III-nitrides: growth, characterization, and properties," *J. Appl. Phys.*, vol. 87, pp. 965–1006, 2000.

[2] D. A. Steigerwald, J. C. Bhat, D. Collins, R. M. Fletcher, M. O. Holcomb, M. J. Ludowise, P. S. Martin, and S. L. Rudaz, "Illumination with solid state lighting technology," *IEEE J. Sel. Top. Quantum Electron.*, vol. 8, no. 2, pp. 310–320, Mar./Apr. 2002.

[3] S. Nakamura, "InGaN-based violet laser diodes," *Semicond. Sci. Technol.*, vol. 14, pp. R27–R40, 1999.

[4] ——, "GaN-based blue/green semiconductor laser," *IEEE J. Sel. Topics Quantum. Electron.*, vol. 3, no. 2, pp. 435–442, Mar./Apr. 1997.

[5] J. S. Im, H. Kollmer, J. Off, A. Sohmer, F. Scholz, and A. Hangleiter, "Reduction of oscillator strength due to piezoelectric fields in GaN/Al_xGa_{1-x}Nquantum wells," *Phys. Rev. B*, vol. 57, pp. R9435–R9438, 1998.

[6] H. K. Cho, J. Y. Lee, C. S. Kim, and G. M. Yang, "Structural and optical investigation of InGaN/GaN multiple quantum well structures with various indium compositions," *J. Electron. Mater.*, vol. 30, pp. 1348–1352, 2001.

[7] S. Nakamura, M. Senoh, S. Nagahama, N. Iwasa, T. Yamada, T. Matsushita, H. Kiyoku, Y. Sugimoto, T. Kozaki, H. Umemoto, M. Sano, and K. Chocho, "InGaN/GaN/AlGaN-based laser diodes grown on GaN substrates with a fundamental transverse mode," *Jpn. J. Appl. Phys.*, vol. 37, pp. L1020–L1022, 1998.

[8] S. Nakamura, M. Senoh, S. Nagahama, N. Iwasa, T. Matsushita, and T. Mukai, "Blue InGaN-based laser diodes with an emission wavelength of 450 nm," *Appl. Phys. Lett.*, vol. 76, pp. 22–24, 2000.

[9] S.-I. Nagahama, M. Sano, T. Yanamoto, D. Morita, O. Miki, K. Sakamoto, M. Yamamoto, Y. Matsuyama, Y. Kawata, T. Murayama, and T. Mukai, "GaN-based laser diodes emitting from ultraviolet to blue-green," *Proc. SPIE*, vol. 4995, pp. 108–116, 2003.

[10] C. Huh, W. J. Schaff, L. F. Eastman, and S.-J. Park, "Temperature dependence of performance of InGaN/GaN MQW LEDs with different indium compositions," *IEEE Electron Device Lett.*, vol. 25, no. 2, pp. 61–63, Feb. 2004.

[11] Y.-K. Kuo and Y.-A. Chang, "Effects of electronic current overflow and inhomogeneous carrier distribution on InGaN quantum-well laser performance," *IEEE. J. Quantum Electron.*, vol. 40, no. 5, pp. 437–444, May 2004.

[12] J.-Y. Chang and Y.-K. Kuo, "Simulation of blue InGaN quantum-well lasers," *J. Appl. Phys.*, vol. 93, pp. 4992–4998, 2003.

[13] O. Mayrock, H.-J. Wünsche, and F. Henneberger, "Polarization charge screening and indium surface segregation in (In,Ga)N/GaN single and multiple quantum wells," *Phys. Rev. B*, vol. 62, pp. 16870–16880, 2000.

[14] G. W. Brown and B. W. Lindsay, "The numerical solution of poisson's equation for two-dimensional semiconductor devices," *Solid-State Electron.*, vol. 19, pp. 991–992, 1976.

[15] T. Ohtoshi, K. Yamaguchi, C. Nagaoka, T. Uda, Y. Murayama, and N. Chinone, "A two-dimensional device simulator of semiconductor lasers," *Solid-State Electron.*, vol. 30, pp. 627–638, 1987.

[16] F. D. Sala, A. D. Carlo, P. Lugli, F. Bernardini, V. Fiorentini, R. Scholz, and J.-M. Jancu, "Free-carrier screening of polarization fields in Wurtzite CaN/InGaN laser structures," *Appl. Phys. Lett.*, vol. 74, pp. 2002–2004, 1999.

[17] C. G. Van de Walle and J. Neugebauer, "Small valence-band offsets at GaN/InGaN heterojunctions," *Appl. Phys. Lett.*, vol. 70, pp. 2577–2579, 1997.

[18] J. Piprek, R. K. Sink, M. A. Hansen, J. E. Bowers, and S. P. Denbaars, "Simulation and optimization of 420 nm InGaN/GaN laser diodes," in *SPIE Proc.*, 2000, vol. 3944-03, pp. 28–39.

[19] S. L. Chuang and C. S. Chang, " k · p method for strained Wurtzite semiconductors," *Phys. Rev. B*, vol. 54, pp. 2491–2504, 1996.

[20] Y. C. Yeo, T. C. Chong, and M.-F. Li, "Uniaxial strain effect on the electronic and optical properties of Wurtzite GaN-AlGaN quantum-well lasers," *IEEE. J. Quantum. Electron.*, vol. 34, no. 11, pp. 2224–2232, Nov. 1998.

[21] L.-H. Peng, Y.-C. Hsu, and C.-W. Chuang, "Structure asymmetry effects in the optical gain of piezostrained InGaN quantum wells," *IEEE J. Sel. Topics Quantum. Electron.*, vol. 5, pp. 756–764, 1999.

[22] C. Juang, K. J. Kuhn, and R. B. Darling, "Stark shift and field-induced tunnelling in $Al_xGa_{1-x}As$/GaAsquantum-well structures," *Phys. Rev. B*, vol. 41, pp. 12047–12053, 1990.

[23] M. Grupen and K. Hess, "Simulation of carrier transport and nonlinearities in quantum-well laser diodes," *IEEE. J. Quantum Electron.*, vol. 34, no. 1, pp. 120–140, Jan. 1998.

Jongwoon Park received the B.S. degree in radio engineering from Kyunghee University, Suwon, Korea, in 1999, the M.S. degree from the University of Victoria, Victoria, B.C., Canada, in 2001, and the Ph.D. degree from McMaster University, Hamilton, ON, Canada, in 2004.

He is currently a Postdoctoral Fellow in the Department of Electronic Science and Engineering, Kyoto University, Kyoto, Japan. His research interests are GaN-based light-emitting devices, fiber-optic communication systems, and numerical modeling and simulation of semiconductor optical devices.

Akio Kaneta received the B.S. and M.S. degrees in electronic and electrical engineering from Gunma University, Gunma, Japan, in 1998 and 2000, respectively, and the Ph.D. degree in electronic science and engineering from Kyoto University, Kyoto, Japan, in 2003.

Since then, he has been working as a Postdoctoral Researcher supported by the 21st Century COE Program of Kyoto University. His current research interest is in the assessment of the optical properties of III–nitride semiconductors by temporally and spatially resolved spectroscopy.

Mitsuru Funato was born in Japan in 1967. He received the B.S. and M.S. degrees in electrical engineering in 1989 and 1991, respectively, and the Ph.D. degree in 2000, all from Kyoto University, Kyoto, Japan. His pH.D. studies focused on GaAs–ZnSe heterovalent heterostructures

He joined at Department of Electrical Engineering, Kyoto University, in 1991 as a Research Associate. In 2000 and 2001, he was a Visiting Research Fellow at the Department of Physics, Heriot-Watt University, Edinburgh, U.K. In 2002, he became a Lecturer at Department of Electronic Science and Engineering, Kyoto University. His current research involves crystal growth and characterization of nitrides.

Yoichi Kawakami was born in Ehime, Japan, in 1961. He received the B.Sc., M.Sc., and D.Sc. degrees in electrical engineering from Osaka University, Osaka, Japan, in 1984, 1986, and 1989, respectively.

After graduation, he joined the Department of Electrical Engineering, Kyoto University as a Research Associate, working on II–VI wide-gap semiconductors. From 1991 to 1992, he was a Visiting Research Fellow with the Department of Physics, Heriot-Watt University, Edinburgh, U.K. In 1997, he became an Associate Professor at the Department of Electronic Science and Engineering, Kyoto University. His current research is focused on spatial and temporal luminescence spectroscopy of excitons in GaN-based low-dimensional semiconductors, as well as on the application of solid-state lighting using white-light-emitting diodes.